

A 2-DOF fMRI Compatible Haptic Interface to Investigate the Neural Control of Arm Movements

R Gassert¹, L Dovat^{2,1}, O Lambercy^{2,1}, Y Ruffieux¹, D Chapuis¹, G Ganesh^{2,3}, E Burdet^{4,2} and H Bleuler¹

¹Laboratory of Robotic Systems, Ecole Polytechnique Fédérale de Lausanne (EPFL), Switzerland

Email: r.gassert@ieee.org http://mrrobotics.epfl.ch

²Department of Mechanical Engineering, National University of Singapore (NUS)

³Department of Cognitive Neuroscience, ATR Computational Neuroscience Laboratories, Japan

⁴Department of Bioengineering, Imperial College London, UK; e.burdet@imperial.ac.uk

Abstract— This paper describes a two-degrees-of-freedom haptic interface to investigate the brain mechanisms of human motor control, which is capable of safely and gently interacting with human arm motion during functional magnetic resonance imaging (fMRI). A hydrostatic transmission separates the interface into a master and an MR compatible slave system, allowing the placement of all interfering components outside the electromagnetic shield of the MR room. The transmission mirrors force and motion of the master actuators on the slave system placed close to the MR scanner. The parallel architecture takes advantage of the linear MR compatible actuators and allows human subjects to perform reaching movements comfortably in the small workspace limited by the dimensions of the MR scanner and the biomechanics of the arm. The kinematic structure of the slave interface was optimized with respect to the available space and types of movements to be investigated. Materials were chosen based on their MR compatibility, their stiffness and weight. The interaction force with the subject is measured over two optical force sensors, located close to the output of the interface. Two shielded optoelectronic encoders measure the extension of the slave hydraulic pistons. Detailed tests demonstrated the fMRI compatibility even during movement of the interface.

I. INTRODUCTION

Over the past few years, functional magnetic resonance imaging (fMRI) has established itself as a major research tool to investigate the brain mechanisms of motor control and cognition. Performing arm movements in controllable dynamic environments during fMRI could provide important insights into human motor control and related dysfunctions, and enable therapists to quantify, monitor, and improve physical rehabilitation. This motivated us to develop fMRI compatible haptic interfaces which can control output force during movements of a human subject and precisely measure position and force while the scanner images the brain [1], [2].

The MR environment demands high safety and electromagnetic compatibility standards, imposing many limits on the development of robotic systems to work in this environment. Several MR compatible robotic systems for interventional MRI [3]–[7] have been developed in the last decade; however, functional MRI is significantly more sensitive to local magnetic field inhomogeneities than diagnostic MRI [2]. Furthermore, while the above systems have to work in the vicinity of the surgeons and patient, they do not need to interact with human

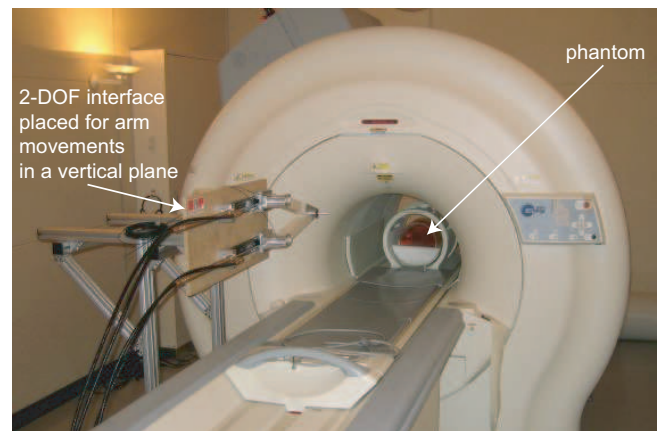


Fig. 1. 2-DOF fMRI compatible haptic interface installed in an MR scanner for phantom compatibility tests at ATR International, Japan.

motion, in contrast to haptic interfaces for neuroscience investigations. This required the development of unconventional solutions for dedicated robotic systems compatible with fMRI and able to produce force and motion safely and gently to interact with the subject's motion [2].

This paper presents the design and extensive compatibility testing of a two-degrees-of-freedom (DOF) haptic interface to study the neural mechanisms of multi-joint arm movements (Fig. 1). It was in particular designed to perform relatively fast reaching movements away from the body over a distance of 20–25 cm. Several studies including [8] have investigated the control of arm movements by measuring position, force and muscle activation (EMG). Our interface will enable the examination of the brain correlates of the observed behaviors.

Section II discusses compatibility issues for such devices and the design constraints of this interface. The design solution is described in section III, its implementation in section IV, and the resulting performances in section V.

II. MR COMPATIBILITY AND MOTION CONSTRAINTS

To be used within an MR environment, a mechatronic device must be MR safe and MR compatible [9], i.e. it must *not*:

- pose a safety threat to the human subject or the scanner,

- disturb the diagnostic or the more sensitive functional imaging, or
- be disturbed by the static magnetic field of typically 1.5 to 3 *Tesla*, the switching magnetic field gradients or the radio frequency (RF) pulses emitted and detected by the scanner, nor be sensitive to any other equipment located in and around the MR room.

Any ferromagnetic components would be strongly attracted by the static magnetic field (missile effect), thus posing a severe safety hazard. Additionally, eddy currents are induced in conducting materials when moving in the fringe-field of the magnet, or by the switching magnetic field gradients, leading to thermal and mechanical effects or even disturbing the imaging. Radiated noise from the scanner or electrical equipment located in the MR or control room can be picked up by cables going from the control room to the mechatronic device, be reemitted by these cables and lead to artifacts on the images.

Most of the MR compatible robotic systems for interventional MRI developed so far [3]–[7] are actuated over ultrasonic motors placed at some distance to the scanner and controlled in position. To our knowledge, none of these systems can perform force-feedback to interact with human motion, and no compatibility tests with functional MRI were reported.

A 1-DOF robot capable of interacting with human wrist motion during fMRI without disturbing the imaging was presented in [10]. This system consists of a master and a slave part, which are electromagnetically decoupled [2]. The slave was realized entirely of polymers and actuated over a hydrostatic transmission. Force-feedback was realized with a fiberoptical sensor based on reflected light intensity measurement. The compatibility of this system is thus independent of the placement or orientation within the MR room and could even be placed within the scanner bore, without disturbing the imaging more than the human subject itself.

The 2-DOF interface presented in this paper will enable us to investigate the neural control of multi-joint arm movements. The design constraints include a workspace of $25 \times 25 \text{ cm}^2$, which must be achieved within the space limitations determined by the dimensions of the MR scanner and the biomechanics of the human arm. In addition, the interface should allow comfortable movements of the subject, it should be as light as possible and strong enough to transmit forces up to 30 *N* in any direction in the movement plane. The hydrostatic transmission we use for actuation has large static friction [11], causing jerk at direction reversals. Therefore, the design should avoid direction reversals in the typical movements that will be investigated, i.e. movement along a straight line with nearly perpendicular force perturbations.

III. CONCEPT

To realize force-feedback with an MR compatible system, we decided to use an actuation principle similar to that of [2], consisting of a master and an MR compatible slave system linked over a hydrostatic transmission. Motion and

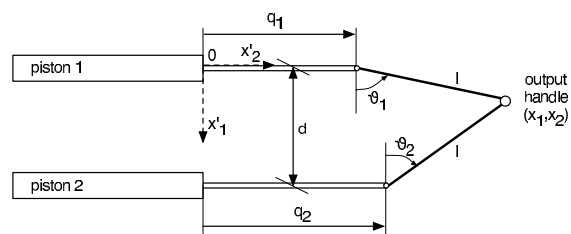


Fig. 2. Schematic of the proposed 2-DOF haptic interface. q_1 and q_2 correspond to the stroke of *piston 1* and *2*, respectively.

force generated by the electromagnetic master actuators can thus be mirrored close to the MR scanner. The optical force sensors allow measurement of the interaction force with the human subject over optical fibers. This principle guarantees electromagnetic decoupling between the MR compatible slave system and the master system located in the control room outside the shield of the MR room.

The 2-DOF haptic interface is conceived to interact with multi-joint arm motion [12]. Due to the location of the arm as well as workspace considerations, it will be placed outside of the imaging region. At the most, the output of the robot will enter into the fringe-field of the scanner. It has been shown that at such distances, non-ferromagnetic metals do not disturb the imaging [13], [14]. As these metals are stiffer and have better surface quality than the polymers used in [10], the components can be scaled down in size, static friction of the hydrostatic transmission can be reduced, and more commercially available components can be used (instead of specially machined polymer parts) in order to optimize system performances. In particular, the high forces that the hand will exert on the handle during experiments require materials with good mechanical properties (i.e. large Young and shear modulae) such as aluminum, brass and zinc.

To improve the dynamic behavior of the system, the inner part of the carriages, which is under less stress, was reduced in size, and the weight of the arms was reduced by using fiberglass profiles, which also guarantees high stiffness.

Kinematic Design and Workspace Analysis

The selected design is shown in Fig. 2. The movement is realized by two carriages with a stroke of 30 *cm* mounted on two parallel guides 15 *cm* apart. Each carriage is actuated by a slave hydraulic piston, connected over two hydraulic pipes to a master piston placed outside the shielded MR room. The two 4 *cm* long and 4 *cm* wide fiberglass arms are connected to the carriages. The closed mechanical chain provides rigidity and allows placing the actuators far from the isocenter of the scanner. The overall system has a length of 87 *cm* to 117 *cm*, a width of 24 *cm* and a height of 15 *cm*.

This design takes advantage of the linear MR compatible actuation capable of performing force-feedback [2] and makes the system compact (Fig. 1). The relative dimensions of the interface, a human subject and the scanner are shown in Fig. 8.

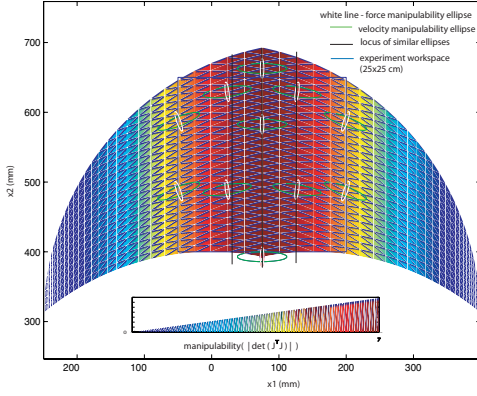


Fig. 3. Manipulability $|\det(\mathbf{J}^T \mathbf{J})|$ of the parallel 2-DOF interface within the square workspace. Velocity manipulability ellipses and force manipulability ellipses are plotted at representative locations, in green and white, respectively.

The kinematic relations were derived using closure constraints. The *inverse kinematics* are given by:

$$\begin{aligned} q_1 &= x_2 - \sqrt{l^2 - x_1^2} \\ q_2 &= x_2 - \sqrt{l^2 - (d - x_1)^2} \end{aligned} \quad (1)$$

with q_1 , q_2 , x_1 , x_2 , l and d as defined in Fig. 2. Note that the terms under the roots are always positive for the selected l and d . The *inverse differential kinematics* are given by:

$$\begin{bmatrix} \dot{q}_1 \\ \dot{q}_2 \end{bmatrix} = \begin{bmatrix} \frac{x_1}{\sqrt{l^2 - x_1^2}} & 1 \\ \frac{x_1 - d}{\sqrt{l^2 - (d - x_1)^2}} & 1 \end{bmatrix} \begin{bmatrix} \dot{x}_1 \\ \dot{x}_2 \end{bmatrix} \quad (2)$$

The direct differential kinematics can be obtained by inverting this relation. As usual with parallel mechanisms, the direct kinematics are more complex. Using closure constraints and trigonometric relations, we obtain the following equations for the *direct kinematics*:

$$\begin{aligned} x_1 &= l \cos \theta_1 = \frac{1}{2}(d \pm q p) \\ x_2 &= q_1 + l \sin \theta_1 = q_1 + \frac{1}{2}(q \pm d p) \end{aligned} \quad (3)$$

where the \pm depends on the position in the workspace, and p and q are defined as:

$$\begin{aligned} q &\equiv q_1 - q_2 = l (\sin \theta_1 - \sin \theta_2) \\ p(q, d) &\equiv \sqrt{\frac{4l^2}{d^2 + q^2} - 1} \end{aligned} \quad (4)$$

This design presents good manipulability over the desired workspace of $25 \times 25 \text{ cm}^2$. Fig. 3 shows the ability of the interface to move in any direction within the desired workspace, indicated by the black square. Simulations with data from real point-to-point movements carried out on a similar (non-MR compatible) 2-DOF interface [8] show that desired movements can be performed with this interface without any direction changes of the actuators during a complete movement (Fig. 4), thus no jerk due to static friction will occur during movement.

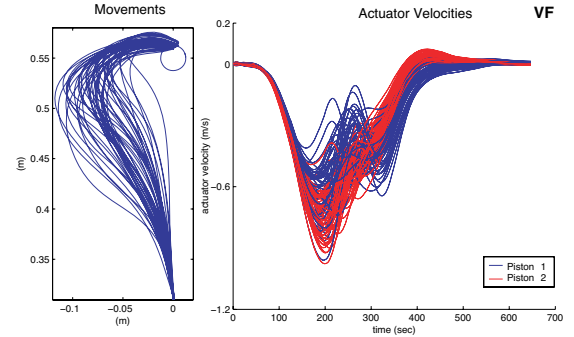


Fig. 4. Plot of 50 reaching movements away from the body in a velocity-dependent rotary force field. The corresponding velocities of the two linear actuators are shown in blue (piston 1) and red (piston 2). The velocities maintain their sign almost throughout the entire movement, thus no motion discontinuity occurs due to static friction. Some movements show sign change of the actuator velocity towards the end of the movement, which is inessential for the projected experiments.

IV. IMPLEMENTATION

A. Design Kinematics

To assure the desired behavior of the 2-DOF interface, it was necessary to consider possible overconstraints. Overconstraint occurs when a joint is blocked due to misalignment between two of the links. Three joints were added to the structure shown in Fig. 2 in order to avoid this (Fig. 5):

- a pair of ball joints, f_2 and f_8 , which avoids overconstraint between the two linear bearings
- a ball joint combined with a plain bearing, f_5 , which avoids overconstraint at the output of the system.

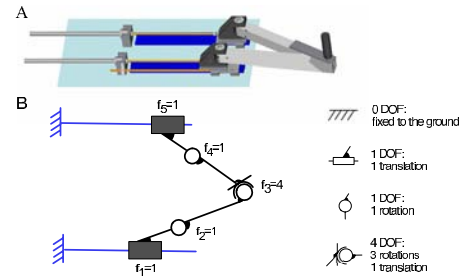


Fig. 5. A: CAD drawing of the 2-DOF interface. B: The number of degrees of freedom of each joint i is represented by f_i . f_1 and f_5 have one translatory DOF, f_2 and f_4 one rotary DOF, f_3 has one translatory and three rotary DOF.

The number of degrees of freedom of the output M can be determined by using Grubler's criterion for closed mechanical chains:

$$M = 6(n - 1) - \sum_{i=1}^l (6 - f_i) \quad (5)$$

where n is the number of links in the system (including the base), l is the number of joints and f_i is the number of degrees of freedom of the i^{th} joint. In our case $n = 5$, $l = 5$ and the number of DOF f_i per joint are shown in Fig. 5, yielding $M = 2$. The kinematic chain has two degrees of freedom and is therefore not overconstrained.

B. Master Actuation Box

The master box contains conventional electromagnetic actuators (EC60 brushless DC motors, Maxon Motor) controlled in current, position or velocity mode over commercially available controllers (EPOS 70/10, Maxon Motor). These actuators are linked to linear axes (ALM 70, Schneeberger) that transmit force and motion to the master hydraulic pistons. Fig. 6 shows the masterbox and its components.

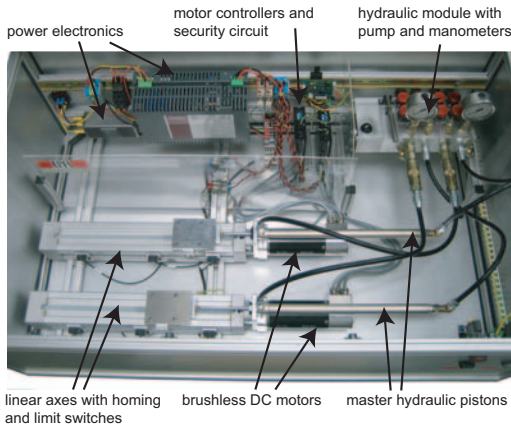


Fig. 6. Master actuation box placed in the control room outside the electromagnetic shield of the MR room. This box contains the master actuators and controllers as well as the hydraulic module. Motion and force are transmitted to the master hydraulic pistons over linear axes. The box measures $100 \times 50 \times 50 \text{ cm}^3$.

C. Optimized Hydrostatic Transmission

The hydrostatic transmission is a critical component of this concept, as it allows actuation of the slave interface and force-feedback without disturbing the imaging, and mainly determines the dynamics of the complete system. The performances of such a transmission are limited by:

- the static friction in the hydraulic pistons. The seals and joints should add little friction, yet close the chambers tightly without leaks.
- the inertia of the oil that needs to be displaced, a column of almost 10 m per line.
- the pipe friction losses and the stiffness of the pipes.

In contrast to [2], we used commercially available brass pistons with non-ferromagnetic (austenitic) steel rods (UVCK-15/300 D, Atec-Cyl SA), leaving out the ferromagnetic nickel plating on the slave pistons. The pistons were selected to have minimal chamber volume but rigid enough rods in order to avoid buckling when the rods are completely extended.

D. Supporting Structure

A rigid aluminium structure was designed to allow placement of the 2-DOF interface in the experimental position to the side of the scanner (Fig. 8) [12]. This structure can be adjusted in height and depth, allowing the subject to perform arm movements in the most suitable position, without touching the scanner bore. If high forces are to be applied to the interface,

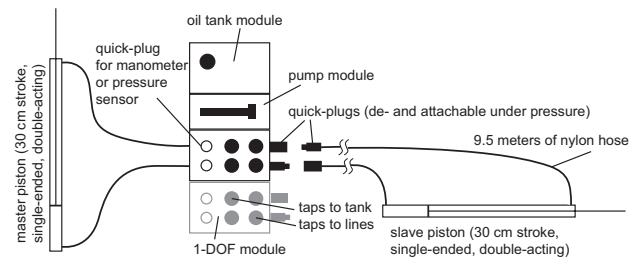


Fig. 7. Schematic of the hydrostatic transmission which links the slave to the master system. A specially developed modular expandable hydraulic module allows pressurization of each chamber of every degree-of-freedom separately. Using the quick-plugs integrated into the hydraulics module, the slave system can be detached and attached from the master system while the lines remain pressurized.

movement of the structure can be prevented by loading the base plate with a water tank.

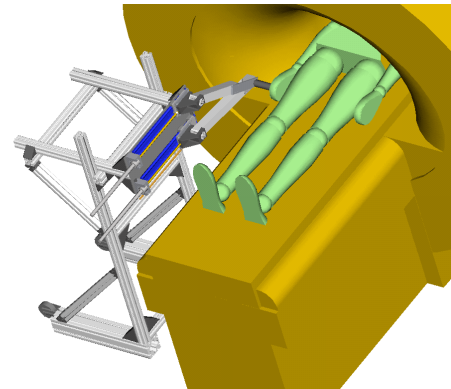


Fig. 8. The 2-DOF interface attached to the supporting structure, placed in the experimental position. The subject inside the MR scanner can interact with the interface during elbow-wrist movements [12]. Other placements of the interface are also possible (e.g. over the body of the subject).

E. Sensors for Force-Feedback

A force sensor is placed in each of the two arms of the MR compatible slave interface so that the force exerted on the handle can be measured through the traction and compression of the two arms joining at the output. The two sensors were placed as close as possible to the output handle in order to minimize sensitivity to parasite torques.

The developed MR compatible force sensor is based on a similar principle as the sensor presented in [15], but improves it in several aspects. The sensing principle is based on optical measurement of the deflection of an elastic body induced by the applied force. Figures 9 and 10 show the optical measurement system.

In contrast to [15], in which the sensor element was milled in a polymer block, the elastic body of our sensor consists of two blades fixed at one extremity to the support (base), and at the other extremity to a moving support (carriage). The optical head is attached to the carriage and the reflective target is fixed to the base over a support shaft. The force applied to the handle

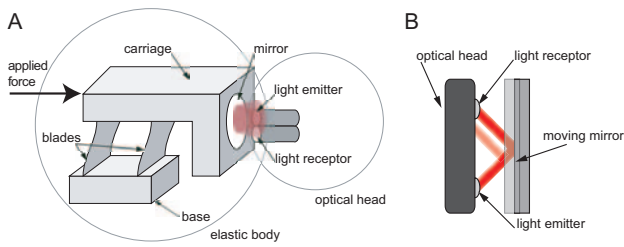


Fig. 9. A: Principle of the definite reflective displacement measurement. B: The reflected light intensity decreases as the reflective target approaches the optical sensor from the focal point.

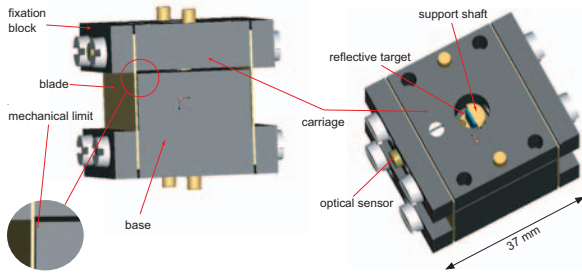


Fig. 10. Design of the optical force sensor integrated into the arms of the haptic interface. An applied force deflects the carriage, leading to a variation in distance between the optical sensor and the reflective target attached to the base. This displacement is measured via reflected light intensity measurement over optical fibers. A mechanical limit prevents plastic deformation of the blades during overload of the sensor.

by the subject deforms the blades and induces a displacement of the carriage. The resulting displacement relative to the base is estimated from the intensity of light reflected on the mirror (Fig. 9B). Note that the blade prevents deformation in other directions, thus minimizing cross-sensitivity. Plastic deformation of the blades is prevented by mechanical limits fixed to the base restricting the travel of the carriage.

This design has several advantages compared to the sensor of [15]:

Compactness The large grooves determined by the diameter of the mill can be reduced, allowing a more compact design.

Accuracy The stiffness of the elastic body is very sensitive to the blade thickness. The tolerances of a laminated blade are smaller than what can be achieved with a milled structure, as used in the design of [15].

Modularity The blades are attached to the structure over a fixation block held by screws, and can thus easily be exchanged to modify the stiffness, i.e. the sensitivity of the sensor.

A drawback of this design, however, is that the assembly must be performed carefully in order to avoid misalignment.

The blade was laser-cut from *CuBe*, a spring material, while polyoxymethylene (POM) was chosen for the base and carriage. The FUE999C1004 optical head (Baumer electric) was preferred to the Keyence FU-38 used in [15] because of

its smaller midrange distance and threaded cylindrical shape, allowing easy fixation and fine-tuning of the distance between the optical head and mirror.

F. Encoders

Transmission stiffness is sufficient to allow direct control of the slave interface through closed-loop position control of the master actuators (with integrated optical encoders); however, position encoders located on the slave can provide accurate measurement useful for psychophysical experiments, and be used to compensate offset between the master and slave pistons.

For the sake of simplicity, and given that the interface is placed outside the scanner bore, we developed specially shielded position encoders using a transparent mask with opaque lines and commercially available position sensors (HEDS 9700, Agilent). To avoid interference between these components and the MR environment, these encoders are shielded and the power lines and data signals are lowpass-filtered in order to remove RF noise (cutoff frequency at 1 MHz) and prevent the scanner from disturbing itself by injecting noise into the cables that is reemitted in the MR environment. Also, as the cables could carry noise from the control room into the MR room, the shield of the encoder cables is linked to the shield of the MR room at the level of the penetration panel, which is connected to the earth, thus providing a stable ground. The RF filter (FP 102, Deltron) is added at the point where the cable is connected to the penetration panel over a D-Sub 9 connector. The encoder chip is placed in a small aluminum box connected to the cable shield.

G. System Control

The master actuators of the interface are controlled by two EPOS 70/10 (Maxon Motor) modules. The communication is realized over a CAN protocol, which allows networking of multiple axis drives, thus requiring only one cable from the control PC to the two axes. The control program was implemented in Labview 7.1 (National Instruments), using the state diagram architecture. The force sensors and encoders are connected to a specially designed data acquisition box, which powers the sensors, filters the signals and feeds them to a data acquisition card (PCI 6221, National Instruments) located in the control computer.

H. Redundant Safety

Interacting with human motion in an MR environment requires a high level of safety. To prevent any harm or damage, both software and hardware emergency systems have been implemented. *In addition* to the safety measures described in [2], this system includes:

- Low-level *security surveillance routines* embedded in the motor controllers. This allows the experimenter to set speed, acceleration and force limitations in advance. If the high-level control generates commands that exceed these limits, the motor controllers will automatically stop

the motors and alarm the experimenter, independent of any malfunction of the high level control.

- A specially designed circuit board that compares the state of all the safety channels, and then activates or deactivates the motor controllers accordingly.

V. PERFORMANCES

A. Force Sensors

During force-feedback, interaction forces with the subject will typically be below 10 N. We therefore chose 15 N as the maximal interaction force. Depending on the position of the interface within the workspace, a force of 15 N applied at the output can lead to a force of up to 45 N on the force sensor. The CuBe blades were thus dimensioned to measure force up to 45 N.

The performances of the two sensors are summarized in Table I. Fig. 11 shows the output of the sensors in function of the applied force. The figure shows good linearity within the range of -30 to 30 N. Even though this range is smaller than the desired 45 N, it is sufficient for preliminary studies and can easily be increased by replacing the blades with thicker ones.

TABLE I
PERFORMANCES OF THE FORCE SENSORS

linear range	± 30.0 N
output range	6.0 V
nonlinearity*	1.2 %
sensitivity	0.1 V/N

* calculated as the maximal output difference to the least square fit, divided by the full-scale output (FSO, Fig. 11)

The difference in force range between the two sensors can be explained by machining and assembly tolerances. Besides the properties of the blade, it is mainly determined by the space between the blade and the mechanical limit as shown in Fig. 10.

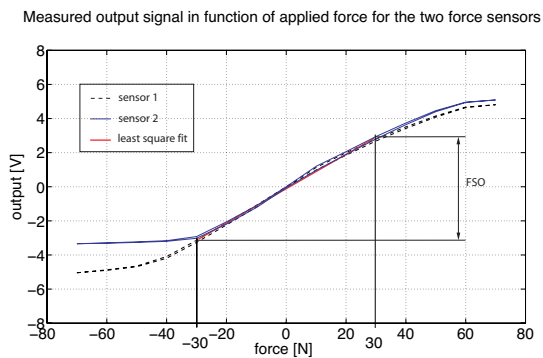


Fig. 11. Output measurement of the two force sensors located in the arms of the interface, showing small hysteresis and good linearity. The superposed line shows a least square fit over the force range of -30 to 30 N.

B. MR Compatibility

MR compatibility of the 2-DOF interface was tested:

- 1) by analyzing the variation of the signal-to-noise ratio (SNR) due to the interface during imaging with respect to a baseline
- 2) by a functional study with a human subject involving a motor task with and without motion of the interface.

All tests were carried out on the same day with a gradient-echo echo planar imaging (GE-EPI) sequence, commonly used in functional MRI, and the same parameters ($TR = 3$ s, $FOV = 224$ mm, 30 slices, $3.5 \times 3.5 \times 3.5$ mm³ voxel size and 1.5 mm gap between slices).

1) *Phantom Tests:* In the first experiment, only the phantom, a plastic cylinder filled with a copper sulphate ($CuSO_4$) solution, was placed inside the MR room. This serves as a baseline for comparison with the tests when the interface is placed in the MR room. A second experiment consisted of two alternating blocks of 24 s length: the interface performed circular motion at constant speed with a radius of 10 cm and a frequency of 1 Hz during the first block, and was at rest during the second block. The signal and signal-to-noise ratio in function of time (Fig. 12) showed no significant difference when the interface was absent, present and at rest, or present and moving. Scans from the different conditions were also inspected visually. Fig. 13 shows that the image of the phantom is not disturbed by the presence and motion of the interface. The subtraction of the two shows that there are no shifts or deformations.

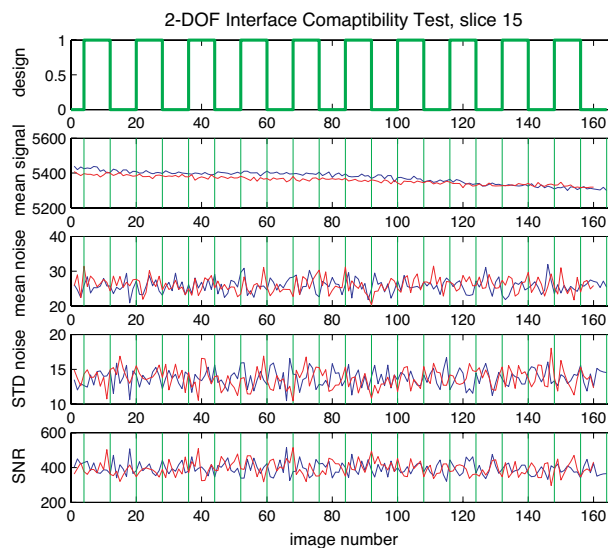


Fig. 12. Results of the phantom compatibility test with the 2-DOF interface. The first row shows the block design, consisting of 4 dummy scans (scanner initialization) followed by 10 repetitions of interface motion (8 scans, 24 seconds) followed by rest (8 scans, 24 seconds). The mean of the signal of a 9×9 voxel square located in the center of the image (row 2) was divided by the standard deviation of a 9×9 voxel square in the upper right corner of the image (STD noise, row 4) to obtain the variation of SNR (row 5). The results (blue) are overlaid on the same values for the measurement with only the phantom (red, the interface was not inside the MR room).



Fig. 13. Phantom scans with the interface at rest (left) and moving (center). The difference (right) shows neither shifts nor deformations.

2) *Functional Study with a Human Subject*: The phantom compatibility tests were completed by a functional study with a human subject. As we eventually want to measure brain activation in motor areas during functional imaging of a motor task, such a task was performed with and without motion of the interface, so that brain activation could be compared. A subject performed alternating 18 s long blocks of finger-tapping and rest. The interface was moved during half of both the rest and finger-tapping blocks, chosen arbitrarily. The MR room was kept completely dark to prevent the subject from perceiving the motion of the interface. Data was analyzed with SPM2 (Wellcome Department of Cognitive Neurology, UCL, London, UK, [16]), a statistical parametric mapping toolbox for Matlab, commonly used for the analysis of functional data [17]. No statistically significant difference was found between the conditions where only finger-tapping was performed compared to those where the interface was also moving, indicating that the imaging is not disturbed by the presence or motion of the interface.

VI. CONCLUSION

This paper presented a novel 2-DOF haptic interface capable of interacting with human arm motion during functional MRI. The interface was designed to allow movements similar to those investigated in [8], taking into account MR safety and compatibility issues as well as the space limitations defined by the dimensions of the MR scanner and the biomechanics of the human arm. The realized MR compatible interface has a workspace of about $25 \times 25 \text{ cm}^2$, can reach velocities of up to 0.3 m/s and generate forces of up to 30 N in any direction.

A rather unusual design procedure was necessary to obtain an interface which does not disturb the imaging and allows subjects to comfortably perform typical movements for the investigation of motor control without generating movement artifacts. This led to a device taking advantage of the linear MR compatible actuators that allow smooth force-feedback during typical reaching movements of about 20 cm within the bore of the scanner. However, movements requiring change of direction in the pistons such as scribbling may suffer from the nonlinearities due to static friction.

To minimize motion artifacts, a supporting structure was realized, which is adjustable and allows placement of the interface so as to interact with arm movements in a vertical plane [12]. Such vertical movements involving the elbow and wrist joints and minimizing shoulder movement seem to create no artifact on the images, in contrast to horizontal arm movements

which involve the shoulder and elbow joints. Preliminary experiments showed that applied forces of 10 N already lead to important shoulder and head movement. This underlines the importance of adapting motor tasks with functional MRI to the MR environment.

While the presented interface was primarily conceived to generate force fields during multi-joint arm movements and observe the brain correlates of motor adaptation to these novel dynamics, it is also very suitable to investigate control of isometric force applied at different positions. In particular, it enables the user to impose a position or trajectory and simultaneously monitor force and position continuously during the imaging. This gives the operator systematic control over the experimental procedure and the possibility to check performance of the subject from the control room.

VII. ACKNOWLEDGMENTS

This work was funded by ATR International, EPFL and NUS. The authors thank Hiroshi Imamizu for his help in defining the requirements of the interface as well as Ichiro Fujimoto and Yasuhiro Shimada for the technical support during the compatibility tests.

REFERENCES

- [1] E. Burdet, *et al.*, "fMRI compatible haptic interfaces to investigate human motor control," *Proc. ISER*, June 2004.
- [2] R. Gassert, *et al.*, "An MRI/fMRI compatible robotic system with force-feedback for interaction with human motion," *IEEE/ASME Transactions on Mechatronics*, April 2006.
- [3] K. Chinzei, *et al.*, "Surgical assist robot for the active navigation in the intraoperative MRI: Hardware design issues," in *Proc. IEEE/RSJ IROS*, 2000, pp. 727–732.
- [4] K. Masamune, *et al.*, "Development of an MRI-compatible needle insertion manipulator for stereotactic neurosurgery," *Image Guid Surg*, vol. 1, no. 4, pp. 242–248, 1995.
- [5] B. Larson, *et al.*, "Design of an MRI-compatible robotic stereotactic device for minimally invasive interventions in the breast," *Journal of Biomechanical Engineering*, vol. 126, no. 4, pp. 458–465, August 2004.
- [6] F. Tajima, *et al.*, "A prototype master-slave system consisting of two MR-compatible manipulators with interchangeable surgical tools," *Proc. IEEE ICRA*, pp. 2505–2510, 2004.
- [7] A. Krieger, *et al.*, "Design of a novel MRI compatible manipulator for image guided prostate intervention," *Proc. IEEE ICRA*, pp. 377–382, 2004.
- [8] E. Burdet, *et al.*, "The central nervous system stabilizes unstable dynamics by learning optimal impedance," *Nature*, no. 414, pp. 446–449, 2001.
- [9] K. Chinzei, *et al.*, "MR compatibility of mechatronic devices: Design criteria," *Proc. MICCAI*, pp. 1020–1031, September 1999.
- [10] R. Moser, *et al.*, "An MR compatible robot technology," in *Proc. IEEE ICRA*, September 2003, pp. 670–675.
- [11] G. Ganesh, *et al.*, "Dynamics and control of an MRI compatible master-slave system with hydrostatic transmission," in *Proc. IEEE International Conference on Robotics and Automation (ICRA)*, 2004, pp. 1288–1294.
- [12] R. Gassert, *et al.*, "Multi-joint arm movements to investigate motor control with fMRI," in *Proc. IEEE EMBC*, 2005.
- [13] J. Schenck, "The role of magnetic susceptibility in magnetic resonance imaging: MRI magnetic compatibility of the first and second kinds," *Medical Physics*, vol. 23, no. 6, pp. 815–850, June 1996.
- [14] R. Gassert, *et al.*, "Active mechatronic interface for haptic perception studies with functional magnetic resonance imaging: Design and compatibility criteria," in *Proc. IEEE ICRA*, 2006.
- [15] D. Chapuis, *et al.*, "Design of a simple MRI/fMRI compatible force/torque sensor," in *Proc. IEEE IROS*, 2004, pp. 2593–2599.
- [16] "SPM2." [Online]. Available: <http://www.fil.ion.ucl.ac.uk/spm>
- [17] R. Frackowiak, *et al.*, *Human Brain Function*, 2nd edition ed. Academic Press, 2003.